Annu. Rev. Phys. Chem. 2000. 51:179–207

PEPTIDES AND PROTEINS IN THE VAPOR PHASE

Martin F. Jarrold
Department of Chemistry, Northwestern University, Evanston, Illinois 60208; e-mail: mfj@nwu.edu

Key Words electrospray, MALDI, FT-ICR, ion mobility, hydration, conformation, helix

■ **Abstract** This article provides a review of recent studies of the properties of unsolvated (and partially solvated) peptides and proteins. The methods used to produce vapor-phase peptide and protein ions are described along with some of the techniques used to study them, such as H/D exchange, blackbody infrared radiative dissociation, and ion mobility measurements. Studies of unsolvated peptides and proteins provide information about their intrinsic intramolecular interactions. The topics covered include the role of zwitterions and salt bridges in the vapor phase, Coulomb interactions in multiply charged ions, the unfolding and refolding of vapor-phase proteins, and the stability of unsolvated helices and sheets. Finally, dehydration and rehydration studies of proteins in the vapor phase are described. These can provide exquisitely detailed information about hydration interactions, such as the enthalpy and entropy changes associated with adsorbing individual water molecules.

INTRODUCTION

With the development of electrospray (1) and matrix-assisted laser desorption and ionization (MALDI) (2), it is now possible to place ions of large biological molecules into the vapor phase. The new soft ionization techniques are sufficiently gentle that as the ions are transferred into the vapor phase, there is usually no fragmentation. Even noncovalently bound complexes can be transferred intact (3–6). These technical developments have revolutionized mass spectrometry and had a profound effect on the life sciences. Determining to within a few Daltons the mass of 50- to 100-kDa proteins or DNA fragments, a feat that would have been virtually impossible before these developments, is now routine (7, 8). The analytical applications extend beyond simple molecular-weight determination. A variety of strategies have been developed to obtain sequence information. Some involve chemical or enzymatic processing in solution (9), whereas others employ the fragmentation of gas-phase ions (true vapor-phase sequencing) (10). It seems likely that in the future, mass spectrometry will find applications in screening for genetic predisposition to disease, in monitoring gene expression (11), and in providing genetic fingerprints.

0066-426X/00/1001-0179$14.00

In addition to applications in bioanalytical chemistry, access to biomolecules in the gas phase provides the opportunity to study them in this environment. The advantage of gas-phase studies is that ideas can be developed and tested on simple model systems. This approach has made important contributions to many areas of chemistry. But is it useful for large biomolecules? There are reasons to believe that it is. The connection between the sequence and three-dimensional structure of a protein, and the mechanism of the folding process itself, are not understood despite decades of study. Nature has engineered the native conformations of most globular proteins to be marginally stable under physiological conditions, so that they are easily denatured by changing the temperature or the solution conditions. Both the intramolecular interactions within the protein itself and interactions between the protein and its solvent are important in defining the native conformation of the proteins. These interactions are large (thousands of kilojoules per mole for a small protein), and both change dramatically during the folding process. But their effects largely cancel out, and under physiological conditions the folding free energy is tens of kilojoules per mole. In solution, folding is effectively driven by the small difference between two large numbers (12, 13). This is why understanding protein structure and folding are such difficult problems, and why they remain unsolved despite decades of solution studies.

By removing a peptide or protein to the vapor phase, it is possible to separate its hydration interactions and intramolecular interactions and examine them independently. For example, studies of secondary structure formation in dehydrated (and partially dehydrated) peptides should provide new insight into the intramolecular (and solvent) interactions that stabilize helices and sheets. In the vapor phase, hydration interactions can be studied essentially one water molecule at a time. ΔH° and ΔS° of hydration can be measured as a function of the number of adsorbed water molecules, and the effects of the adsorbed water on the conformation of the protein can be examined. The use of computer simulations to study biological molecules has been expanding rapidly (14, 15). Because so many atoms are involved, these simulations almost always employ simple empirical force fields for both the intramolecular and the hydration interactions. It is not surprising that the accuracy of the potential energy functions have been questioned (16). The results of studies of unsolvated and partially solvated peptides and proteins should prove useful in refining and testing these theoretical models.

MALDI AND ELECTROSPRAY

If a biological sample is heated, it decomposes before it vaporizes, and no molecular ions are observed (except possibly some very small ones). One way around this problem is to deliver the energy to the system very quickly, so that large molecular ions desorb before they are cooked. Sputtering-based methods such as fast atom bombardment (17), ^{235}Cf plasma desorption (18), and pulsed-laser desorption (19) are all realizations of this approach. Systematic studies of pulsed-laser desorption have shown that the best results are obtained with lasers in the far-ultraviolet,

where resonant absorption occurs. These studies revealed an upper limit of around 1000 Da for biopolymers, which presumably results from photodissociation. The breakthrough to higher masses came with the realization that dissociation could be circumvented with a matrix. The analyte is diluted (at around 1 part in 100–50,000) in a solid or liquid matrix that strongly adsorbs the laser light (2). Matrices are usually large organic acids such as 2,5-dihydroxybenzoic acid. The matrix disperses the analyte, preventing oligomer formation, and enhances ionization of the analyte through proton transfer from photoexcited matrix molecules. One of the strengths of MALDI is that the resulting ions are predominantly singly charged. However, the signal intensity decreases with increasing mass, presumably because it is still difficult to get large molecules airborne even with the matrix. The signal depends on the morphology of the sample being irradiated. Efforts to avoid the use of an organic matrix include excitation under surface plasmon resonance conditions (20) and the use of porous silicon as a substrate (21).

In electrospray (1), a solution of the biomolecule is effused through a small capillary held at several kilovolts relative to an electrode a few centimeters away. The high electric field at the end of the capillary pulls the solution into a Taylor cone. If the field is strong enough to overcome surface tension, the cone is drawn to a filament that generates small charged droplets. It has been suggested (22) that free molecular ions are formed by a series of droplet fissions caused by solvent evaporation (as a charged droplet shrinks, it eventually reaches the Rayleigh limit, where the electrostatic forces overcome the surface tension holding the droplet together and it breaks apart). Another view is that the ions evaporate directly from small, highly charged droplets under the influence of Coulomb repulsion (23). The relative importance of these two processes remains a topic of research and discussion. Ion production continues as the electrosprayed droplets are transferred from ambient pressure to the high vacuum conditions normally associated with mass spectrometers. The interface typically consists of a short, heated capillary tube followed by a differentially pumped skimmer. The capillary tube is heated to promote dehydration. In "normal" electrospray, a metal capillary tube is used as the emitter, and the solution is delivered by a syringe pump at 3–20 μl/min. Higher sensitivity and stability are obtained with "microelectrospray," which employs flow rates of $\sim$500 nl/min and a narrow-bore (50 μm), fused silica capillary as the emitter (24). "Nanospray," with an electroosmotic flow of $\sim$50 nl/min and an emitter with an orifice diameter of 1–2 μm, requires very small samples (25).

SOME PROPERTIES OF ELECTROSPRAYED IONS

Unlike MALDI, which generates mainly singly charged ions, electrospray tends to produce ions with mass-to-charge ratios of around 500–2500 Da. This means that the ions of even small proteins such as bovine pancreatic trypsin inhibitor (BPTI) (58 residues, 6511.6 Da) and bovine cytochrome *c* (104 residues, 12229.1 Da) are multiply charged. A distribution of positive charge states ranging from +4 to

+7 is observed for BPTI. The charge results from the addition of protons to basic sites to yield $[M + nH]^{n+}$. The main positive ion observed for BPTI under most conditions is +6. Negative ions (resulting from deprotonation of acidic residues) can be obtained by reversing the polarity of the high voltage on the emitter.

The formation of multiply charged ions is an advantage because the mass-to-charge ratio of large ions falls within the normal range of a quadrupole mass spectrometer. However, ions with masses of hundreds of kilodaltons, which can be produced by electrospray (26), have hundreds of charges and a broad distribution of charge states. This spreads the signal over many peaks, reducing the signal-to-noise ratio, and makes mixture analysis difficult. Schemes have been developed to reduce the charge down to singly charged ions (27, 28). There is no upper limit to the mass of an ion that can be produced by electrospray. Individual coliphage T4 DNA ions with masses around 10^8 Da and with around 30,000 charges have been observed using Fourier transform ion cyclotron resonance (FTICR) (29).

Solution conditions can affect the charge-state distribution observed for protein ions (30). The charge-state distribution measured for bovine cytochrome *c* with an unacidified aqueous solution (pH = 5.2) peaks around +10, the distribution recorded at pH = 3.0 is bimodal with maxima at +8 and +16, and at pH = 2.6 there is a single distribution centered around +16. These changes have been attributed to changes in the solution-phase conformation. Bovine cytochrome *c* is in a folded conformation in an unacidified aqueous solution, whereas it is denatured (unfolded) in a highly acidic solution. The increase in the number of charges that occurs when cytochrome *c* unfolds has been attributed to the unfolded protein exposing more basic sites for protonation. Such dramatic changes in the charge-state distribution are not observed with BPTI, which has three disulfide bonds that prevent it from adopting a fully unfolded conformation. It has often been suggested that there is a rough correlation between the charge on electrosprayed ions and the overall charge in solution. However, recent studies of protein-charge ladders show no correlation (31). Partial acetylation of the primary amine groups (N terminus and lysine side chains) was used to prepare a series of proteins with different overall charge in solution. Electrospray mass spectra of the series were not significantly different. It is often possible to account for the maximum charge state of electrosprayed ions by considering proton transfer to the solvent (32, 33). As the charge increases, Coulomb repulsion within the $[M + nH]^{n+}$ ion increases, and it becomes more acidic. Ultimately, the acidity increases to the point where the ion can transfer a proton to a solvent molecule, and then higher charge states are not observed.

METHODS FOR STUDYING VAPOR-PHASE PEPTIDES AND PROTEINS

Relatively few techniques can be used to obtain structural information for large ions in the vapor phase. Those that can be include chemical methods like H/D exchange; dissociation studies, from which some structural information has been

deduced; and methods based on measurements of size, such as ion mobility. FTICR (34, 35) is a versatile technique that has been used in many chemical reactivity and dissociation studies of vapor-phase peptides and proteins. In FTICR, the ions are trapped under high vacuum conditions ($<10^{-8}$ torr) in an ICR cell (a box consisting of three pairs of metal plates) by a combination of electric and magnetic fields. A strong magnetic field in the *z*-directions constrains the ions to undergo cyclotron motion in the *xy* plane while voltages on the trapping plates along the *z* direction prevent the ions from escaping. The mass is determined from the cyclotron frequency. The ions are coherently excited by a radio frequency signal applied to the pair of plates along the *x* direction, and the decay of the image current is observed on the pair of plates along the *y* direction. FTICR provides high mass resolution and high mass accuracy. The equivalent of unit mass resolution has been achieved for a 112-kDa protein (8). Coupling an external electrospray source to an FTICR instrument is a challenge because of the magnetic mirror effect that occurs as ions are transferred into a region of high magnetic field (36). An assortment of ion guides and electrostatic lenses have been devised to overcome this problem (37, 38). While stored in the ICR cell, the ions can be exposed to a variety of reagents, low-energy collisions, or light of various wavelengths. Only a low pressure of a reagent or a collision gas can be employed; however, this is more than compensated for by trapping times of up to $\sim$1 h.

In the low-pressure environment of an FTICR cell, internal equilibrium is attained primarily through adsorption and emission of infrared photons. Weakly bound ions may be driven to dissociate by the radiation field (39, 40). Large ions equilibrate with the radiation field faster than they dissociate (this is equivalent to the high pressure limit for unimolecular reactions) (41), and thus Arrhenius activation energies can be determined from measurements of dissociation rates as a function of the temperature of the ICR cell (up to $\sim$200°C). This approach, which is now called blackbody infrared radiative dissociation (BIRD) (41), has been used to determine activation energies in the range of 50–150 kJ mol^{-1}.

As an alternative to the more "chemical" methods of deducing structural information, several groups have employed physical methods based on determining the size or collision cross section. An unusual example of this approach is provided by the work of a group at Uppsala University (42–44). They used atomic force microscopy and scanning tunneling microscopy to examine the defects generated by the high-energy impact of multiply charged protein ions on graphite. Low charge states of myoglobin produced by electrospraying an unacidified solution gave nearly circular defects, whereas the defects generated by the higher charge states of apomyoglobin (from an acidified solution) were elongated, and became more elongated as the charge increased. Ion beam scattering has been used to measure the collision cross sections of protein ions (45–48). The cross sections of cytochrome *c* ions increase with increasing charge (45). For intermediate charge states, the cross sections depended on the nature of the electrosprayed solution, which indicates that the ions retain a memory of their solution-phase structure (45).

Ion mobility measurements provide a more accurate method for determining collision cross sections. The mobility is a measure of how rapidly an ion moves through a buffer gas under the influence of a weak electric field, and it depends on the ion's average collision cross section with the buffer gas. The measurements are performed in a drift tube, which contains the buffer gas (which is usually several Torr of helium) and has a uniform electric field along its length. The minimum experimental configuration consists of a source and drift tube, followed by a quadrupole mass spectrometer and detector. A packet of ions is injected into the drift tube, and the different conformations separate as they travel through it. At the other side of the drift tube, some of the ions exit, and they are mass analyzed and detected. Drift-time distributions are obtained by measuring the ions' arrival time distribution at the detector. The separation, or resolving power, depends on the voltage drop across the drift tube (49). High-resolution ion mobility measurements, incorporating drift voltages of up to 14 kV, have been described (50, 51).

The use of a transport property to deduce structural information in the gas phase dates back to 1925 (52, 53), when diffusion constants were used to probe the structures of simple molecules such as anthracene. In the 1970s and 1980s, several groups demonstrated that ion mobilities could be used to resolve structural isomers of gas-phase ions (54, 55). But it was the work that used mobilities to examine the structures of carbon cluster ions (56) that sparked the recent interest in this approach. Deducing structural information from mobilities (or diffusion constants) requires calculation of the average collision cross sections for trial geometries for comparison with the experiment results. A variety of schemes have been developed, ranging from a simple projection approximation (which uses the geometric cross section) (52, 57) to methods based on trajectory calculations (58). The projection approximation underestimates the cross sections for large ions because it does not treat the scattering process properly (59). Mobility measurements can be performed as a function of drift-tube temperature to study conformational changes. Conformational changes (or dissociation processes) can also be driven by raising the injection energy so that the ions are collisionally heated as they enter the drift tube (60). Reactions such as water adsorption and H/D exchange can be studied by adding reagents to the buffer gas in the drift tube. There is also considerable interest in developing the separations capabilities of ion mobilities, which may have applications in analyzing protein digests and peptide libraries (61, 62).

SELF-SOLVATION, ZWITTERIONS, AND SALT BRIDGES

The gas-phase basicity (GB) and proton affinity are defined as $-\Delta G$ and $-\Delta H$ for the reaction $[M + H]^+ \rightleftarrows MH^+$. GBs have been measured for individual amino acids and a variety of small peptides (63, 64). Three amino acids (arginine, lysine, and histidine) have basic side chains that are often protonated in vapor-phase

peptides and proteins. For lysine and histidine, the high GBs are partly due to strong intramolecular interactions, whereas arginine has the very basic guanidine group. Some other amino acids (glutamine, proline, and tryptophan, for example) have slightly basic side chains that may be protonated in the gas phase. The N terminus and backbone amide groups may also be protonated. Quantum chemical calculations indicate that protonation at the amide CO group is preferred to protonation at the NH (65). The GBs of peptides usually increase with increasing chain length. This results from "self-solvation," where the protonated group interacts with other electronegative groups; hydrogen bonds between the pronated group and backbone carbonyl groups are thought to be the most important interaction (66–69). Similar self-solvation interactions are expected in unsolvated protein ions. In solution, the basic groups (which tend to be on the surface of proteins) extend out into the solvent when protonated, whereas in the gas phase they are expected to fold back and self-solvate.

Electrostatic interactions are the main long-range interaction in biomolecules, and they play a major role in defining the structure and properties. Electrostatic interactions are stronger in the vapor phase than in solution because they are not attenuated by the solvent. Water has a dielectric constant of 78 and it effectively solvates and stabilizes charge. Zwitterions, for example, are much less prevalent in the vapor phase than in solution. In aqueous solution, amino acids exist predominantly as zwitterions (NH_3^+-CHR-COO^-) instead of the neutral form (NH_2-CHR-COOH). It was established some time ago that the neutral form of glycine is preferred in the vapor phase (70, 71). Calculations suggest that as few as two water molecules may be enough to stabilize zwitterionic glycine (72); however, this interesting result has not been confirmed experimentally. Spectroscopic studies of jet-cooled tryptophan have been interpreted as indicating that it forms a zwitterion in an electronically excited state (73). Amino acids with acidic or basic side chains are more likely than glycine to form ground-state zwitterions in the vapor phase (74). However, even the very basic arginine appears to favor the neutral form in the gas phase (75). For a protein in aqueous solution at pH $\sim$ 7, acidic side chains are usually deprotonated and basic ones protonated. For hen egg white lysozyme, for example, all 17 arginines and lysines are protonated and all 10 carboxylic acids are deprotonated, giving a net charge of $+7$. In the gas phase, where ions are not solvated by water, the neutral state is preferred, except for residues that must be protonated (or deprotonated) to account for the overall charge.

A salt bridge (a charged group arrangement of $+\ -\ +$ or $-\ +\ -$) is another common type of electrostatic interaction. There is mounting evidence that salt bridges are important for unsolvated proteins and peptides. BIRD studies (76) suggest that the lowest energy form of bradykinin (Arg-Pro-Pro-Gly-Phe-Ser-Pro-Phe-Arg) $[M + H]^+$ has a salt bridge where both arginine side chains are protonated and interact with the deprotonated C terminus carboxyl group. Activation energies were measured for the dissociation of a variety of bradykinin analogs. Of particular note, methylation of the C terminus carboxylic acid (which blocks salt bridge formation) decreases the activation energy for dissociation from 1.3 eV to

0.6 eV. A similar approach has been used to argue that a salt bridge occurs in the proton-bound dimer of arginine (74). Here both guanidine groups are protonated and one of the carboxyl groups is deprotonated. The charged arginine effectively stabilizes a zwitterion in the uncharged one. Salt bridges have also been invoked as intermediates in H/D exchange (77) and in the fragmentation of sodiated peptides (78). Sodiated peptides undergo selective cleavage at aspartic acid residues when collisionally excited. This was rationalized by a mechanism where the sodium ion stabilizes the ion pair formed by proton transfer from the aspartic acid to the adjacent amide nitrogen. Ion mobility measurements and theoretical studies using quantum chemical methods and density functional theory indicate that neither protonated (Gly_nH^+) nor sodiated (Gly_nNa^+) ($n \leq 7$) polyglycines adopt salt-bridge structures (79).

In multiply charged protein ions, Coulomb interactions between the charges become important and can strongly influence the properties, including the fragmentation (80), proton transfer reactions (81), and conformations (45). Because of their long range, Coulomb interactions often lead to the formation of a reverse activation barrier to processes involving charge separation. The barrier results because as the charges are brought together, the Coulomb energy becomes substantial before it can be overcome by shorter-range attractive interactions. In some cases this can lead to a metastable bound state lying above the energy of the fragments (82).

PROTON TRANSFER REACTIONS AND APPARENT GAS-PHASE BASICITIES

The GB of a multiply charged ion is defined by $-\Delta G$ for the reaction

$$[M + (n-1)H]^{(n-1)+} + H^+ \rightleftarrows [M + nH]^{n+}. \qquad 1.$$

For proton transfer from a multiply charged ion,

$$[M + nH]^{n+} + B \rightarrow [M + (n-1)H]^{(n-1)+} + BH^+, \qquad 2.$$

there is a reverse activation barrier in the exit channel (due to Coulomb interactions), and the reaction may not occur even if it is thermodynamically allowed. Because of the reverse activation barrier, bracketing studies (where one tries to deduce the GB of $[M + (n-1)H]^{(n-1)+}$ by examining the proton transfer reactivity of $[M + nH]^{n+}$ with known bases) yield an apparent GB (GB^{app}) that is larger than the true value (a stronger base is needed to remove a proton from $[M + nH]^{n+}$ than would be required in the absence of the barrier]. However, the Coulomb energy within the $[M + nH]^{n+}$ ion increases with increasing charge. The increased Coulomb energy makes the ion more acidic, and the GB^{app} decreases with increasing charge, despite the activation barrier. Although the terms GB and GB^{app} are

widely used in the present context, what is really measured in these experiments is the apparent gas phase acidity (GA) of the $(M + nH)^{n+}$ ion. The GA is ΔG for the reaction

$$(M + nH)^{n+} \rightleftarrows [M + (n-1)H]^{(n-1)+} + H^{+}. \qquad 3.$$

Note that $GA\{[M + nH]^{n+}\} = GB\{[M + (n-1)H]^{(n-1)+}\}$. GB^{app}s (or more correctly GA^{app}s) have been determined for a variety of multiply charged peptide and protein ions. Kinetic studies of the proton transfer reactions of the $[M + 12H]^{12+}$ ion of ubiquitin (a small protein with 76 residues) revealed two populations that react at significantly different rates (83). These two populations were attributed to different conformations of the $[M + 12H]^{12+}$ ion. Valentine et al (84) have performed combined ion mobility/proton transfer studies of ubiquitin. They found that the proton transfer reactivity was ordered as compact conformations > partially folded > elongated, as would be expected from consideration of the Coulomb energies (84).

Williams and collaborators (85–88) have suggested that the difference between the GB^{app} and the intrinsic basicity of the site that is protonated (the GB of that site in the absence of the other charges) can be related to the Coulomb energy of a multiply charged ion. Thus, the Coulomb energy is written as

$$\sum_{ij} \frac{q_i q_j}{4\pi\epsilon_0\epsilon_r r_{ij}} \approx GB^{intrinsic} - GB^{app} + T\Delta\Delta S, \qquad 4.$$

where $\Delta\Delta S$ is the difference in ΔS for protonating the neutral protein and the protein with $n-1$ charges. For the $[M + 2H]^{2+}$ ion of gramicidin S (a cyclic decapeptide), the measured GB^{app} and $GB^{intrinsic}$ were used along with a value for r_{ij} derived from molecular dynamics (MD) simulations to estimate a value of 1.2 for the dielectric constant (ϵ_r). Using a similar approach, a dielectric constant of 1.01 ± 0.07 was found for a series of doubly protonated 1,n-diaminoalkanes ($n = 7$–10, 12). However, this analysis has been questioned (89). The right hand side of Equation 4 ignores the reverse activation barrier in the exit channel of Equation 2, and consequently it underestimates the Coulomb energy. Taking the barrier into account leads to $\epsilon_r < 1.0$. Gronert (90) has shown that $\epsilon_r < 1.0$ can result from the point charge approximation (used in Equation 4). This neglects delocalization and overestimates the charge separation (90). However, there is also a problem with bracketing GB^{app}, which depends on determining whether or not proton transfer occurs. For multiply charged ions, the transition between reactive and unreactive bases is not sharp, making the choice of the threshold and the assigned GB^{app} somewhat arbitrary (89, 91).

For a protein with N protonation sites, n of which are protonated, there are $N!/n!(N-n)!$ different ways of protonating the sites. For even a small protein like cytochrome *c*, the number of different charge permutations is enormous and it is not easy to determine which sites are protonated. This issue was first considered by Schnier et al (87), who estimated the energy of the different charge permutations

from

$$E = \sum_{ij}^{n} \frac{q^2}{4\pi\epsilon_0\epsilon_r r_{ij}} - \sum_{i}^{n} \mathrm{GB}^{\mathrm{intrinsic},i}, \qquad 5.$$

where the first term results from Coulomb interactions between the protonated sites and the second term is the sum of the intrinsic GBs of the sites that are protonated. A more sophisticated approach that evaluates self-solvation and charge dipole interactions for each site has been described (92). But both schemes ignore the conformational changes that occur in response to the protonation of a particular set of sites, and so they overestimate Coulomb repulsion. Mao and coworkers (93) have used the preceding scheme to identify low-energy-charge permutations, which were then relaxed to allow conformational changes.

GB^{app}s measured for cytochrome *c* $[M + 3H]^{3+}$ to $[M + 15H]^{15+}$ have been analyzed using Equations 4 and 5 and, assuming a fully denatured (linear) structure, yield a value of $\epsilon_r = 2.0 \pm 0.2$ (87). There is considerable interest in knowing the dielectric constant within proteins (94–96). However, the value found here may not be as reliable as indicated. Ion mobility measurements for cytochrome *c* have subsequently shown that the low charge states (+6 and below) are almost as compact as the native conformation (97). GB^{app}s measured for hen egg white lysozyme (98) and a dielectric constant of 2.0 have been used to deduce information about the conformations of disulfide-intact (DI) and disulfide-reduced (DR) lysozyme ions in the vapor phase (lysozyme has four disulphide bonds). The GB^{app}s determined in these studies are plotted in Figure 1. GB^{app}s were calculated for X-ray crystal structure coordinates and for a fully denatured one-dimensional string. The measured GB^{app} of the high charge states (+11 to +15) of DR lysozyme fit those calculated for the fully denatured form, whereas the low charge states of both the DR and DI are closer to those calculated for the crystal structure. Below +8, both forms have similar proton transfer reactivities. This was interpreted as indicating that the DR ions (which were denatured in solution) refold in the vapor phase. The main conclusions of this study are supported by ion mobility measurements (see below) (99).

Coulomb interactions also have a strong influence on the dissociation energies and fragmentation patterns of multiply charged ions. A reverse activation barrier (due to Coulomb interactions) develops in the exit channel as the charge increases, but highly charged ions are still expected to dissociate more readily than those with fewer charges (80). A simple "charges on a string" model was used to investigate the Coulomb effects on the dissociation of highly charged ions (80). The model predicts that as the charge increases, the rate of dissociation at sites toward the center of the string increases relative to those toward the ends (80). Measured product distributions are a strong function of the charge state, and in some cases charge state–specific fragmentation processes have been found (100). The dissociation of gas-phase protein ions has received a considerable amount of attention because it can be used to provide sequence information. A number of methods

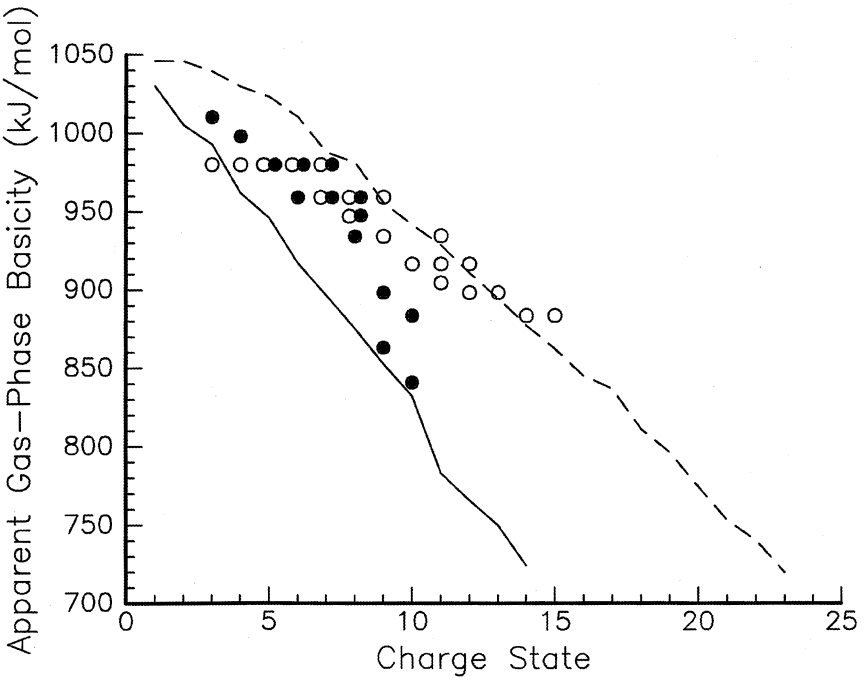

Figure 1 GB^{app} of $[M + (n - 1]H)^{(n-1)+}$ (measured by proton transfer from $[M + nH]^{n+}$) for disulphide-intact (*filled circles*) and disulphide-reduced (*open circles*) hen egg white lysozyme as a function of charge state. Calculated GB^{app}, modeled using X-ray crystal structure coordinates (*solid line*) and as a fully denatured one-dimensional string (*dashed line*), are shown for comparison. (Adapted from Reference 98.)

have been described, including collision-induced dissociation with a buffer gas, photodissociation, surface-induced dissociation, thermally activated dissociation, and electron capture dissociation (101–108). Most methods yield mainly *b* and *y* fragments (R-CO and NH-CHR′) from cleaving the amide bond, although electron capture dissociation produces mainly *c* and *z* fragments (RC(OH)=NH and CHR′). In general, dissociation occurs at sites adjacent to acidic or basic residues. Some preferred fragmentation points have been identified: the C-terminal side of aspartic acid (109); the N-terminal side of prolines, particularly those with adjacent acidic residues (110); and at a lysine at the N-terminal side of a histidine. Several studies support the prediction that increasing the charge lowers the dissociation energy of multiply charged ions (102, 104, 111). However, for the fragmentation of the +5 to +11 charge states of ubiquitin, Arrhenius activation energies (from BIRD studies) appear to increase with increasing charge (105). A curious feature of these results is the strong correlation between the Arrhenius activation energy and the preexponential factor (see Table 1). Ion mobility measurements for

TABLE 1 Arrhenius activation parameters for the dissociation of the +5 to +11 charge states of ubiquitin[a]

Charge state	E_a, eV	Log A
+5	1.16 ± 0.06	12.0 ± 0.7
+6	0.93 ± 0.04	9.2 ± 0.7
+7	0.99 ± 0.03	9.4 ± 0.3
+8	1.20 ± 0.07	11.8 ± 0.8
+9	1.21 ± 0.05	12.0 ± 0.6
+10	1.55 ± 0.11	16.3 ± 1.0
+11	1.55 ± 0.06	16.7 ± 0.7

[a]From Reference 105.

ubiquitin show multiple conformations for the +5 to +8 charge states and a transition from compact to elongated geometries ongoing from the +5 to +11 charge state (84). It is not clear how the presence of several conformations affects the BIRD results, but the unfolding transition may explain why the dissociation energies do not decrease with increasing charge.

H/D EXCHANGE IN THE VAPOR PHASE

In solution, H/D exchange has been widely used to deduce structural information, and more recently it has been used to probe protein folding (112, 113). Several groups have employed H/D exchange to examine proteins in the gas phase (83, 114–120). As in solution, it is assumed that hydrogens buried in the core of a folded protein exchange much less readily than do those on the surface. McLafferty and coworkers have reported several H/D exchange studies of protonated cytochrome *c* using FT-ICR (115, 116, 118). The ions are trapped for long times while exposed to a small partial pressure of D_2O, and then the number of labile hydrogens is obtained from the mass spectrum. Figure 2 shows the number of protein H atoms exchanged (from the total exchanged minus the number of charges) for $(M + 6H)^{6+}$ to $[M + 19H]^{19+}$. Eight exchange levels were found for some charge states, ranging from ∼56 to ∼134. Equine cytochrome *c* has 198 exchangeable hydrogens, 144 of which are exchanged in 20 min by the native conformation in a neutral solution. The systematic decrease in the exchange level as the charge increases (see Figure 2) was attributed to the self-solvation shell around each charge, protecting sites that would otherwise undergo exchange. Transitions between some of the exchange levels (presumably unfolding and refolding) were induced by infrared laser heating, by collisional heating and cooling, or by reducing the number of charges. The

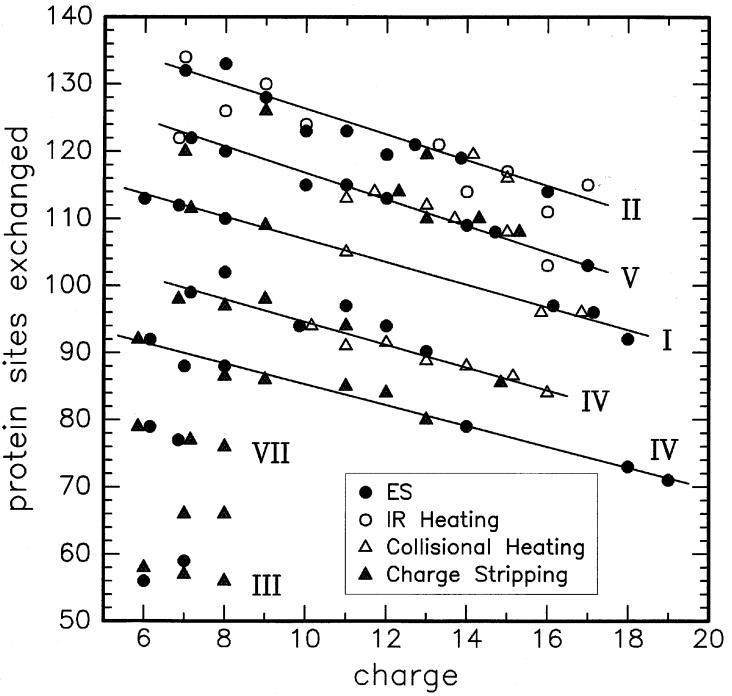

Figure 2 Plot of the number of protein H atoms [excluding the protons added by electrospray (ES)] that are exchanged by 10^{-7} torr of D_2O in 30 min for ions formed by ES (*closed circles*), infrared (IR) laser heating (*open circles*), charge stripping (*closed triangles*), and quadrupolar axialization with N_2 followed by ion cooling (*open triangles*). (Adapted from Reference 118.)

observation of many exchange levels for the +7 and +8 charge states is consistent with ion mobility studies where five conformers were resolved for these ions (97). However, for the higher charge states (>+9), only a single peak was observed in the ion mobility measurements, and the cross sections increase with increasing charge while the exchange levels decrease. It appears that in the vapor phase, more extended structures do not necessarily result in more extensive H/D exchange.

Valentine & Clemmer have used drift-tube methods to study H/D exchange in different cytochrome *c* conformations (117). The injection energy into the drift tube was adjusted to prepare conformations with different cross sections. Only two exchange levels were found: 45–48 for folded conformations with cross sections of 1260–1510 $Å^2$, and 60–65 for unfolded ones with cross sections of 2130–2770 $Å^2$. The difference between the exchange levels found here and in the FT-ICR experiments may be related to the different timescales. Although the ions in both

experiments experience roughly the same number of collisions with D_2O, FTICR has a much longer timescale than the drift-tube experiments. The cytochrome *c* ions may undergo slow conformational changes, which expose more labile hydrogens in the longer FTICR experiments.

H/D exchange has been studied in amino acids and small peptides (77, 121–123). The results suggest that the interpretation of gas-phase H/D exchange data for even simple systems is not straightforward. For example, Gly_nH^+ with $n = 2$ exchanges all labile hydrogens with D_2O, whereas $n = 1$ and $n > 3$ do not undergo facile exchange. On the other hand, Gly_nH^+, where $n = 1$–5, exchanges all labile hydrogens with ND_3 (77). H/D exchange in small monofunctional compounds is known to proceed efficiently when the difference between the GBs of the reagent and deprotonated analyte molecule is small. The drop in exchange reactivity with D_2O for $n > 3$ was attributed to the substantial difference between the GBs of the larger Gly_n peptides and D_2O (ND_3 has a larger GB and so the difference is smaller). A number of exchange mechanisms were considered. Of particular note is the relay mechanism proposed for exchange with D_2O (77). Because D_2O is not very basic, mechanisms involving simple H-bond formation or salt-bridge intermediates are unfavorable. The relay mechanism requires two basic sites with similar GBs to be in close proximity. The more basic site should be protonated. H^+ and D^+ are shuttled between the sites via the water molecule to effect the exchange. Wyttenbach & Bowers (124) have used the relay mechanism to model H/D exchange between bradykinin $[M + H]^+$ and D_2O. Bradykinin $[M + H]^+$ was assumed to have the salt-bridge structure described above. Their model considered surface accessibility of the protonated arginines and the backbone amide groups and the distance between them. Good agreement with experiment was achieved by averaging over an ensemble of low-energy conformations. In more recent FT-ICR studies, bradykinin $[M + H]^+$ was found to undergo much less exchange than had previously been found (<0.5 D were incorporated after exposure to D_2O at 10^{-5} torr for 1 h) (125). The exchange observed in previous studies was attributed to collisional heating of the ions. Campbell et al (77) have indicated that the relay mechanism should be disfavored in peptides containing basic residues like arginine because of the disparity in functional group basicities (in this case arginine and the backbone amide groups). This may partly account for the low exchange rates found for bradykinin $[M + H]^+$ in the more recent studies. Note that the $[M + H]^+$ ion of O-methylbradykinin (which cannot form a salt-bridge structure and has only one of the arginines protonated) very rapidly exchanges all 17 labile hydrogens, whereas the O-methylbradykinin $[M + 2H]^{2+}$ ion (with both arginines protonated) exchanges none. Freitas & Marshall concluded that these results support the salt-bridge structure for bradykinin $[M + H]^+$ (125). Little work has been done with chemical probes other than H/D exchange. Stephenson et al (126) have found that the kinetics of HI attachment differ significantly for native and DR BPTI. HI is expected to attach to (unprotonated) basic sites, and this chemistry may provide a complimentary structural probe to H/D exchange (126).

ION MOBILITY STUDIES OF PROTEIN UNFOLDING AND REFOLDING

Ion-mobility measurements have been performed for a variety of proteins, including BPTI (51, 97), cytochrome *c* (51, 93, 97, 127), apomyoglobin (128), lysozyme (99), and ubiquitin (84). The conformations present depend on the charge state and the conditions employed. Cross sections for the resolved conformations of cytochrome *c* are plotted against charge in Figure 3. The low charge states have collision cross sections close to the value calculated for the crystal structure coordinates, whereas the high charge states have cross sections close to that expected for an extended string. The unfolding transition that occurs between the +5 and +10 charge states is driven by Coulomb repulsion, and it is somewhat analogous to acid-induced denaturation in solution. Conformational changes can be induced by collisional heating as the ions enter the drift tube (60). At low injection energies the +7 and +8 charge states remain folded, but when the injection energy is raised they unfold. Conformational changes can also be induced by changing the temperature of the drift tube: Raising the drift-tube temperature to 300°C causes

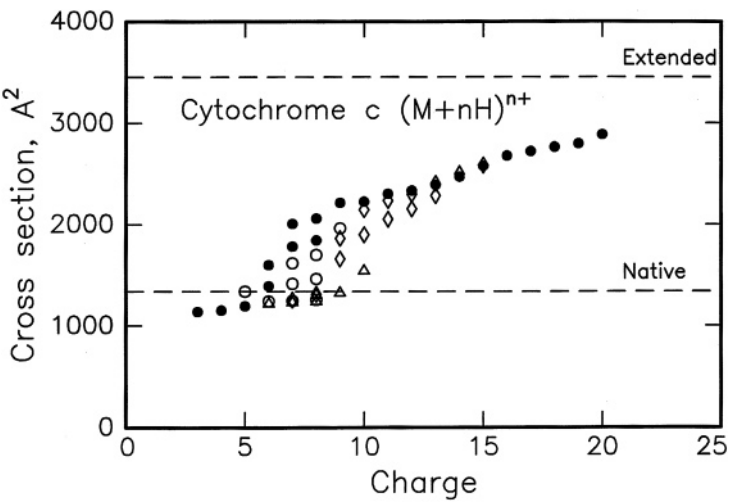

Figure 3 Plot of the cross sections of the main features resolved in the drift time distributions of the +3 to +20 charge states of bovine cytochrome *c*. Cross sections are shown for features observed on an injected ion drift tube apparatus at high injection energies (*closed circles*) and for metastable conformations observed at lower injection energies (*open circles*). Features observed on a high-resolution apparatus (with no injection energy) are also shown. Here the cross sections depend on the electrosprayed solution. Results are shown for an unacidified aqueous solution (*open triangles*) and for an acidified solution (*open diamond*). (*Dashed lines*) The cross sections calculated for the crystal structure coordinates and for a fully extended string.

a slight increase in the cross section measured for the +5, but the +7 undergoes a series of unfolding transitions (93). In the absence of collisional heating, the room-temperature drift-time distributions for the +7 to +10 depend on the nature of the electrosprayed solution. Ions produced from an unacidified aqueous solution (native), 1:1 water and methanol (methanol denatured), and acidified solutions (acid denatured) can be distinguished (51). The low charge states of cytochrome *c* (<6+) are not made directly by electrospray. The +3 to +5, for which cross sections are shown in Figure 3, were obtained from higher charge states by proton transfer to bases added to the desolvation region. These ions have compact folded conformations even when they are produced from unfolded, high charge states generated by electrospraying an acidified solution. This indicates that the protein ions refold in the vapor phase. In some cases, for example apomyglobin $(M + 6H)^{6+}$, there is an activation barrier (presumably a Coulomb barrier) to refolding, and refolding only occurs after the ions are collisionally heated (129).

Lysozyme is slightly larger than cytochrome *c* (129 versus 104 residues), and it has four disulphide bonds whereas cytochrome *c* has none. Cross sections determined for the main features observed in the drift-time distributions of DI and DR hen egg white lysozyme are shown in Figure 4 (99). Electrospray of DI lysozyme yields +8 to +11, whereas +10 to +18 are formed for DR. Lower charge states were produced by proton transfer reactions. Only unfolded conformers (at >2400 Å^2) are present for the +10 to +18 DR ions formed by electrospray. Folded (at ∼1300 Å^2) and partially unfolded conformations are present for DI lysozyme. Obviously, the disulphide bonds prevent the DI ions from unfolding all the way. The lower charge states of DR lysozyme produced by proton transfer from the unfolded, higher charge states have cross sections that indicate they have refolded or partially refolded.

Results have been reported for MD simulations of the unfolding and refolding of lysozyme ions in the gas phase (129–132). Unfolding was studied by a repulsive centrifugal potential and by Coulomb forces due to multiple protonation. To effect denaturation, a higher charge was required in the simulations than appears necessary in the experiments. Unfolding and refolding trajectories of (neutral) lysozyme were analyzed by plotting them on a map of anisotropy against entanglement (132). It was argued that the refolding trajectories were not random because they involved a simultaneous decrease in the anisotropy and an increase in the entanglement. Figure 5 shows an example of one of the refolding trajectories. This trajectory becomes trapped in a local minimum, with the anisotropy and entanglement some distance from simulations started from the crystal structure (marked by IVNS in Figure 5). Mao and coworkers (133) have performed MD simulations of the unfolding and refolding of cytochrome *c*. These simulations reproduced the threshold for charge-induced unfolding observed in ion-mobility studies, but they underestimate the degree of unfolding for the intermediate charge states. Representative conformations from the MD simulations for the +9 and +19 are shown in Figure 6. The +9 remains folded, whereas the +19 almost completely unfolds. Calculated cross sections for these conformations are close

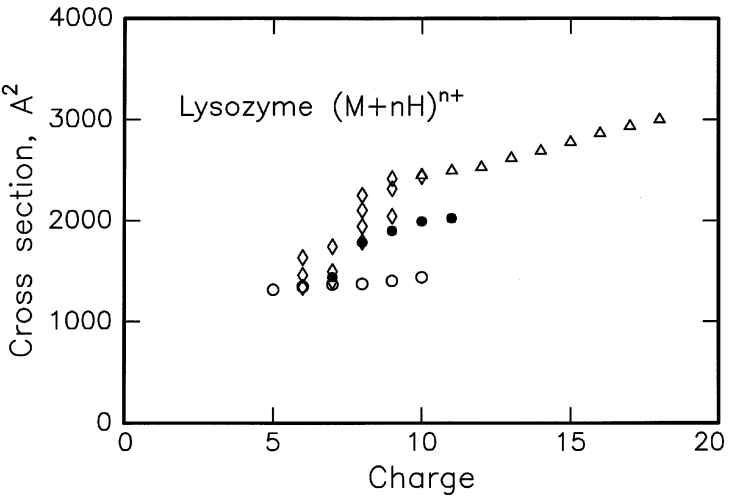

Figure 4 Plot of the cross sections of the main features resolved in the drift time distributions of disulphide-intact (DI) and disulphide-reduced (DR) lysozyme. Cross sections obtained at high (*filled circles*) and low (*open circles*) injection energies are shown for DI. For DR, cross sections are shown for +10 to +18 ions derived directly from electrospray (*open triangles*) and for lower charge states generated by proton transfer reactions from the higher charge states (*open diamond*). (Adapted from Reference 99.)

to the measured cross sections. Refolding was examined by removing protons from unfolded $[M + 19H]^{19+}$ ions. The $[M + 9H]^{9+}$ ions generated by removing 10 protons were much less compact than the +9 conformations generated by starting the simulations from the crystal structure (see Figure 6). However, the energies of the folded and partially refolded +9 conformations are similar. This shows how flat the energy landscape is for the intermediate charge states. The flattening of the energy landscape by electrostatic interactions has been used to explain why, as the temperature is raised, the +7 charge state unfolds while the +5 remains folded (93). Removing another six charges from the $[M + 9H]^{9+}$ ions to give $[M + 3H]^{3+}$ ions results in further collapse (see Figure 6), but the final geometries were substantially less compact, and significantly higher in energy, than the +3 charge states started from the crystal structure (which have similar conformations to the folded +9 in Figure 6). Similar nonspecific collapse has been found by Alonso & Daggett in MD simulations of ubiquitin refolding in solution (134).

SECONDARY STRUCTURE IN UNSOLVATED PEPTIDES

A large fraction of the amino acids in proteins are in α-helices or β-sheets, and thus there is great interest in the factors that are responsible for the stabilities of these secondary structure units. There have been many studies of helix formation in

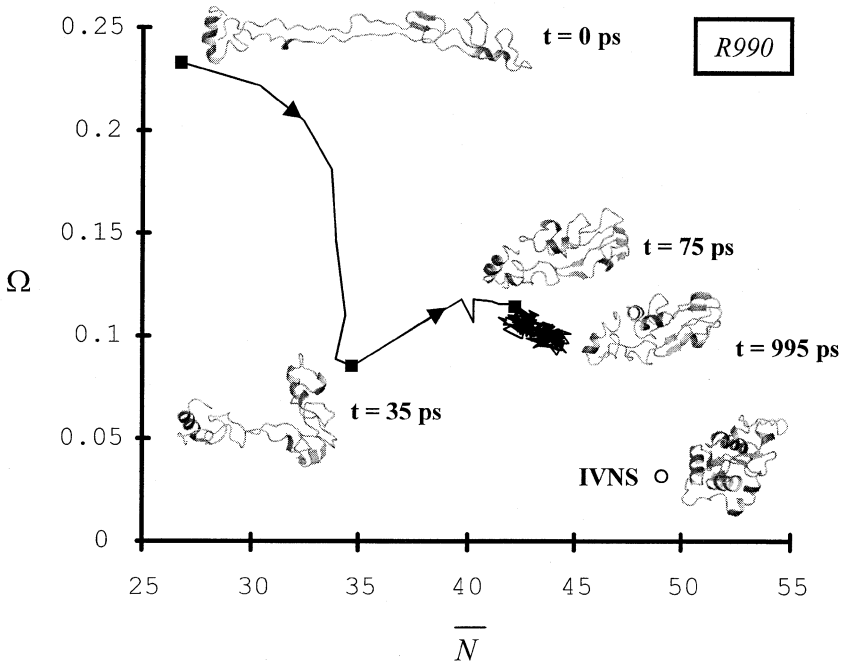

Figure 5 Map of anisotropy (Ω) and entanglement ($\bar{N}$) for one of the refolding trajectories of neutral disulphide-intact lysozyme. (*Black squares*) The positions of the snapshots. The snapshot labeled IVNS is for a simulation starting from the crystal structure coordinates. (Reproduced with permission from Reference 132.)

solution, and they have provided some insight into the factors responsible for helix stability (135). A thermodynamic scale of the helix propensities of the different amino acids has been established. β-Sheets are much less well understood. A β-hairpin, consisting of a turn and a short length of anti-parallel sheet, can be viewed as a model fragment of a β-sheet. The first β-hairpin that is stable as a monomer in solution has only recently been discovered (136).

Studies of α-helix and β-sheet formation in unsolvated peptides should provide a deeper insight into the role of the solvent and intramolecular interactions in stabilizing secondary structure. Kaltashov & Feneslau (137) have used mass-analyzed ion kinetic energy spectrometry to examine the conformation of melittin, a 26-residue peptide that is helical in solution. The structure of the $[M + 3H]^{3+}$ ion was probed by measuring the kinetic energy released in its metastable dissociation (unimolecular fragmentation on a microsecond timescale). It was assumed that the kinetic energy release was related to the Coulomb repulsion between the charges, and that it could be used to provide a measure of the inter-charge distance. By comparison with the inter-charge distances determined from MD simulations,

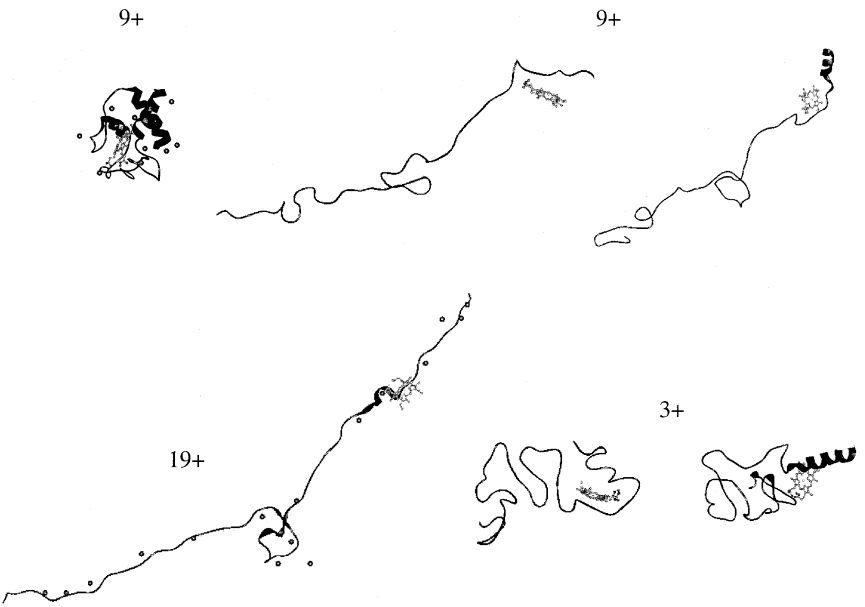

Figure 6 Representative conformations from the molecular dynamics simulations of cytochrome *c* ions in vacuo; (*Left*) The folded +9 and unfolded +19 are from simulations started from the crystal structure. (*Dots*) The location of the charges. The partially refolded +9 conformations were produced by removing 10 protons from the unfolded +19. They are more compact than the +19 and are much less compact than the folded +9 prepared from the crystal structure, although the partially refolded and folded +9 have similar energies. The +3 conformations were prepared by removing an additional six protons from the +9. These are less compact than the folded +3 generated from the crystal structure and are significantly higher in energy.

it was concluded that melittin probably retains its helical conformation in the gas phase. Although ingenious, there are several concerns with this approach. First, fragmentation on a microsecond timescale probably involves temperatures that are above those usually associated with the stability of secondary structure. Second, the measurements probe the kinetic energy release as the products separate from the transition state, and the transition state may have a structure that is different from that of the stable conformation. The same approach has been used to examine β-sheet formation in the gas phase (138). It was concluded that a 12-residue de novo design β-hairpin (139) and the 33-residue βpep-4 peptide (140), which forms a three-strand β-sheet in solution, both retained their conformations in the vapor phase.

Ion-mobility measurements (141) and MD simulations (142) have been used to examine helix formation in protonated polyalanine (Ala_nH^+) and polyglycine (Gly_nH^+) peptides with up to $\sim$20 residues. In solution, glycine has a low helix

propensity, whereas alanine has the highest of the natural amino acids (135). In the gas phase, both oligopeptides adopt random globular conformations where the rest of the peptide appears to wrap up around the charge and "solvate" it by hydrogen bonds to backbone carbonyl groups. MD simulations of Ala_nH^+ peptides started as helices rapidly collapse to random globular conformations, whereas simulations for neutral Ala_n persist as helices. In the Ala_nH^+ peptides, the charge is believed to be located at the N terminus. An α-helix has a macrodipole that results from the alignment of the backbone NH and CO groups. The positive end of the macrodipole is at the N terminus, and placing a positive charge there destabilizes the helix. Hudgins and coworkers have designed a stable gas-phase helix by acetylating the N terminus and placing a lysine at the C terminus to carry the charge (143, 144). Ion-mobility measurements show that the resulting Ac-Ala_n-$LysH^+$ peptide is a helix with as few as eight residues, whereas its analog with the lysine at the N terminus, Ac-$LysH^+$-Ala_n, adopts a random globular conformation. Representative structures from MD simulations of Ac-Ala_{19}-$LysH^+$and Ac-$LysH^+$-Ala_{19} are shown in Figure 7. In the Ac-Ala_{19}-$LysH^+$ peptide, the protonated lysine side chain wraps around and caps the end of the helix by hydrogen bonding to the dangling carbonyl groups. For the Ac-$LysH^+$-Ala_n peptides, the random globular conformation is only observed up to $n = \sim 13$. For $n > 13$, (Ac-LysH-$Ala_n)_2^{2+}$ dimers dominate. These dimers are believed to have the conformations shown in Figure 7*c*. Here the protonated lysine at the N terminus of one peptide interacts with the C terminus of the other to form an antiparallel head-to-toe helical dimer. The dimerization process is driven by the stability of the helices.

Studies of the glycine analogs, Ac-Gly_n-$LysH^+$ and Ac-$LysH^+$-Gly_n, have also been performed (145). Ac-Gly_n-$LysH^+$ and Ac-$LysH^+$-Gly_n both have mobilities that are close to those expected for random globules. Thus, when subjected to the same stabilizing features that lead to helix formation in alanine peptides, the glycine peptides do not form helices. The behavior of the unsolvated peptides appears to parallel the behavior in solution, where alanine has a high helix propensity and glycine has a low one. However, one should not assume that vapor-phase helix stabilities always track the solution-phase propensities. Recent studies of valine-based peptides suggest that valine helices are even more stable in the vapor phase than alanine helices. In aqueous solution, valine has a helix propensity that is only slightly higher than that of glycine.

An attempt is being made to develop sequence-structure relationships in small peptides. Collision cross sections have been recorded for 660 peptides with 4–24 residues derived from tryptic digests (146). The cross sections for subsets containing 3–5, 5–10, and 10–15 residues were analyzed to obtain intrinsic size parameters: the relative contribution of the individual amino acid to the measured cross sections. Somewhat different contributions were found from the different subsets. However, contributions derived from measurements for small oligomers are in good agreement with those obtained for similar-sized peptides.

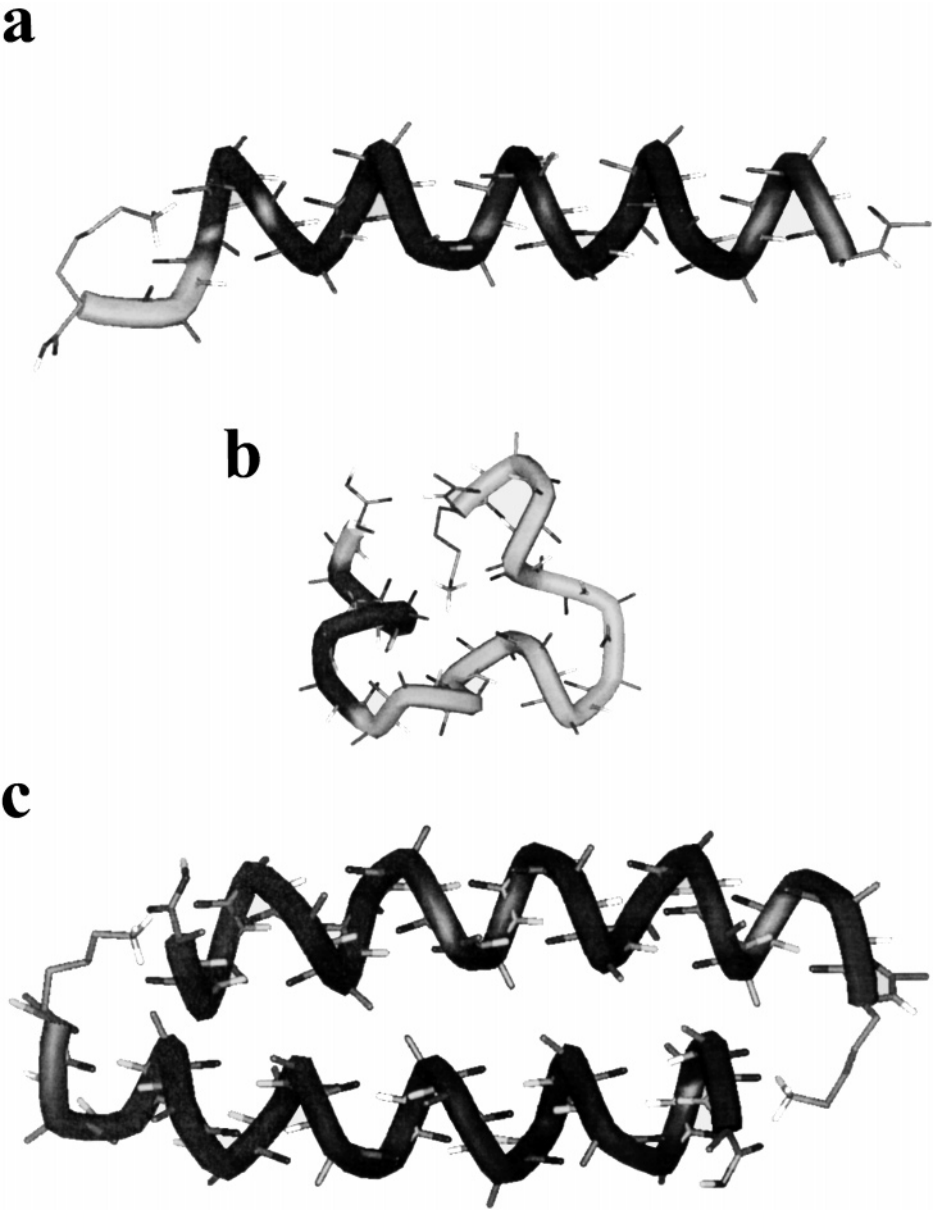

Figure 7 Representative structures from molecular dynamics simulations: (*a*) Ac-Ala_{19}-$LysH^+$ helix; (*b*) Ac-$LysH^+$-Ala_{19} random globule; and (*c*) $(Ac\text{-}LysH\text{-}Ala_{19})_2{}^{2+}$ antiparallel head-to-toe helical dimer. (Reproduced with permission from Reference 14.)

HYDRATION AND DEHYDRATION OF VAPOR-PHASE PEPTIDES AND PROTEINS

Vapor-phase proteins provide new opportunities to study the important issue of protein hydration. In the past, mass spectrometry–based techniques have been widely used to study the first stages in the solvation of monoatomic and polyatomic ions (147). There are two basic ways to examine hydrated proteins in the gas phase: Leave water on the protein ion when it is produced or add water to a dehydrated protein. Several groups (148–151) have used the first approach. They operated their electrospray sources so that the protein ions were not completely dehydrated. Rodriguez-Cruz et al (149, 150) have reported mass spectra measured for "wet" gramicidin S $[M + 2H]^{2+}$ ions. The intensities of the peaks due to ions with 8, 11, and 14 water molecules were enhanced relative to their neighbors, indicating that ions with these numbers of water molecules are favored for some reason. It was suggested that 8, 11, and 14 water molecules correspond to stable solvation shells around both of the charge sites on the ion. Lee et al (151) have used FTICR to examine hydrated peptides generated by electrospray. Over time, they undergo a "freeze-drying" process, where they evaporate water and cool. This process is expected to result in a temperature of around 130–150 K from a balance between evaporative cooling and heating by blackbody radiation. A prominent peak in the mass spectrum due to gramicidin S $[M + 2H]^{2+}$ with 40 water molecules was ascribed to a structure where both protonated ornithine residues are solvated by 20 water molecules in a pentagonal dodecahedral clathrate structure. This structure has previously been proposed to explain a prominent peak observed in the mass spectrum of protonated water clusters (152). In contrast to gramicidin S, mass spectra for hydrated bradykinin $[M + 2H]^{2+}$ did not show any prominent peaks.

The other approach to studying protein hydration is to start with a dehydrated protein ion in the gas phase and to rehydrate it by exposing it to water vapor. The number of adsorbed water molecules can be determined by mass spectrometry, and if equilibrium is established, equilibrium constants can be determined. An equilibrium constant measured at a single temperature provides ΔG° for hydration at that temperature. But equilibrium constants measured as a function of temperature provide ΔH° and ΔS°. If these thermodynamic quantities can be obtained as a function of the number of adsorbed water molecules, they can be used to follow the development of the hydration shell. Previously, thermodynamic information about protein hydration has been obtained from studies of the hydration of protein films (153, 154). However, the information obtained from these studies is affected by hysteresis. Furthermore, only average values can be obtained by this method. Klassen et al have determined hydration-free energies for several small peptides (155). They found that ΔG° at 293 K for binding the first water to Gly_nH^+, where $n = 1$–4, were 41, 37, 28, and 24 kJ mol^{-1}. The substantial decrease between Gly_2H^+ and Gly_3H^+ was attributed to cyclization and intramolecular self-solvation of the charge site. Zhan et al have described preliminary results obtained for the

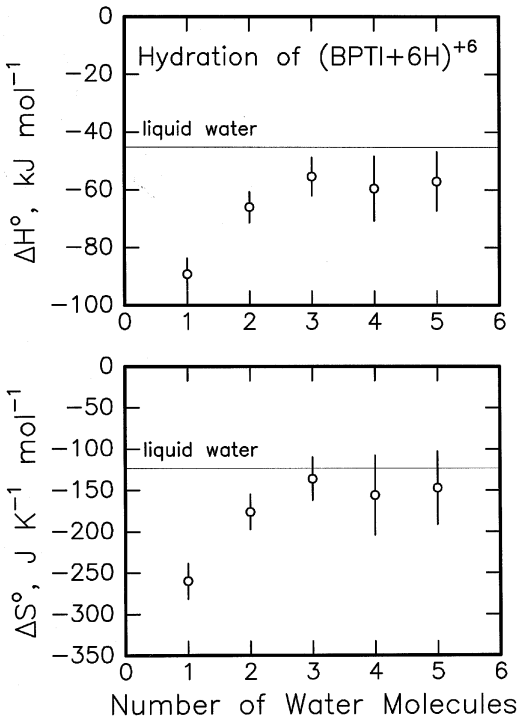

Figure 8 ΔH° and ΔS° for the adsorption of the first few water molecules on BPTI $[M + 6H]^{6+}$ (BPTI, bovine pancreatic trypsin inhibitor). (*Solid lines*) Show ΔH° and ΔS° for transferring a water molecule from the gas phase to the liquid phase. (Adapted from Reference 158.)

solvation of the peptide leucine-enkephalin with water and a variety of alcohols in a free jet expansion (156).

Woenckhaus and coworkers have measured ΔG° at 273 K for initial steps in the rehydration of the $[M + 5H]^{5+}$ and $[M + 7H]^{7+}$ charge states of cytochrome *c* (157). Temperatures significantly below room temperature were required to see any water stick to the protein ions. ΔH° and ΔS° have been determined for the first few water molecules adsorbed on the $[M + 6H]^{6+}$ charge state of BPTI (see Figure 8) (158). ΔH° and ΔS° for the fourth and fifth water molecules have a large uncertainty associated with them because their equilibrium constants were only measured over a narrow temperature range. ΔH° and ΔS° for adsorption of the first water molecule onto BPTI are substantially more negative than for subsequent water molecules. It was originally suggested (158) that the first water molecule went into a conserved structural water site on BPTI (W122) (159, 160). However, MD simulations suggest that this is not a stable hydration site for the unsolvated BPTI $[M + 6H]^{6+}$ ion (the water molecule migrates out of this site and solvates a protonated arginine that is nearby) (161). According to the simulations, the first water is probably tetrahedrally coordinated at another site within the protein (a site that is not hydrated in the crystal). Tetrahedral coordination of the water was found to stiffen the low-frequency modes of the protein. This causes

a significant decrease in the vibrational entropy when the water is adsorbed and explains the large entropy change for adsorption of the first water molecule.

The average number of water molecules adsorbed under near saturation conditions (with a water vapor pressure close to the equilibrium vapor pressure) has been determined for a number of cytochrome *c* and apomyoglobin charge states (162). For cytochrome *c*, around 50 waters adsorb on the folded +4 and +5 charge states (with 0.73 torr of water vapor at -20°C). For the unfolded +7 to +12 charge states, the number of water molecules adsorbed under the same conditions drops to below 30. A similar sharp decrease in the number of adsorbed waters is observed at the unfolding transition for apomyoglobin. One would expect the number of water molecules adsorbed by the unfolded conformations to be larger than the number adsorbed by the folded ones. Solvation energies of proteins are usually estimated from an accessible surface area model (163). The experimental observations clearly conflict with the predictions of this model. This suggests that cooperative effects, where water molecules interact simultaneously with more than one site on the protein, are important in the hydration of the folded conformation. When the protein unfolds, it is more difficult to interact with multiple sites.

As described above, ion-mobility measurements indicate that a charge-induced unfolding transition occurs around the +7 charge state of unsolvated cytochrome *c* (see Figure 3). In solution, charge states up to around +11 remain folded (164). Thus, if water molecules are added to unfolded $[M + 7H]^{7+}$ ions in the gas phase, at some point they should fold and adopt the solution-phase conformation. Fye et al have examined this issue (162). There are two peaks present in the drift-time distribution for the unfolded +7 charge state in the absence of the water, and as the number of adsorbed water molecules increases, the distribution shifts over to the more folded conformation at shorter time. The addition of only 29 water molecules is apparently enough to promote this refolding. More water molecules are needed to drive the +7 charge state to a completely folded conformation, but at this point it is not clear how many more are needed.

PROSPECTS

The developments that provide access to vapor-phase peptides and proteins are relatively recent, and so far only a few techniques have been used to characterize them. The hydration studies are particularly important because, in addition to their intrinsic interest, they provide a link between the vapor phase and the solution phase. It is clear that better structural information is required. One direction for future work is the application of spectroscopic methods. Traditional high-resolution spectroscopy may not find many applications, but methods based on fluorescence quenching have been successfully used in solution studies of peptides and proteins, and they should work in the vapor phase as well. Virtually all the work described in this article has been on peptide and protein ions where Coulomb interactions seem to play an important and perhaps often a controlling role. Thus, even though they

are more difficult to study than ions, it is also desirable to study neutral peptides and proteins. Some important properties, for example dipole moments, can only really be measured for neutral peptides and proteins.

Visit the Annual Reviews home page at www.AnnualReviews.org

LITERATURE CITED

1. Fenn JB, Mann M, Meng CK, Wong SF, Whitehouse CM. 1989. *Science* 246: 64
2. Hillenkamp F, Karas M, Beavis RC, Chait BT. 1991. *Anal. Chem.* 63:1193A
3. Smith RD, Bruce JE, Wu QY, Lei QP. 1997. *Chem. Soc. Rev.* 26:191
4. Przybylski M, Glocker MO. 1996. *Angew. Chem. Int. Ed. Engl.* 35:806
5. Vogl T, Roth J, Sorg C, Hillenkamp F, Strupat K. 1999. *J. Am. Soc. Mass Spectrom.* 10:1124
6. Gao J, Wu Q, Carbeck J, Lei QP, Smith RD, Whitesides GM. 1999. *Biophys. J.* 76:3253
7. Chait BT, Kent SBH. 1992. *Science* 257: 1885
8. Kelleher NL, Senko MW, Siegel MM, McLafferty FW. 1997. *J. Am. Soc. Mass Spectrom.* 8:380
9. Chait BT, Wang R, Beavis RC, Kent SB. 1993. *Science* 262:89
10. McLuckey SA. 1992. *J. Am. Soc. Mass Spectrom.* 3:599
11. Paša-Tolić L, Jensen PK, Anderson GA, Lipton MS, Peden KK, et al. 1999. *J. Am. Chem. Soc.* 121:7949
12. Lazardis T, Archontis G, Karplus M. 1995. *Adv. Protein/Chem.* 47:231
13. Makhatadze GI, Privalov PL. 1995. *Adv. Protein/Chem.* 47:307
14. Duan Y, Kollman PA. 1998. *Science* 282: 740
15. MacKerell AD, Bashford D, Bellott M, Dunbrack RL, Evanseck JD, et al. 1998. *J. Phys. Chem. B* 102:3586
16. Beachy MD, Chasman D, Murphy RB, Halgren TA, Friesner RA. 1997. *J. Am. Chem. Soc.* 119:5908
17. Barber M, Bordoli RS, Sedgwick RS, Tyler AN. 1981. *J. Chem. Soc. Chem. Commun.* 1981:325
18. MacFarlane RD, Torgerson DF. 1976. *Science* 191:920
19. Posthumus MA, Kistemaker PG, Meuzelaar HLC, ten Neuver de Brauw MC. 1978. *Anal. Chem.* 50:985
20. Owega S, Lai EPC, Bawagan ADO. 1998. *Anal. Chem.* 70:2360
21. Wei J, Buriak JM, Sluzdak G. 1999. *Nature* 399:243
22. Dole M, Mack LL, Hines RL, Mobley RC, Ferguson LD, Alice MB. 1968. *J. Chem. Phys.* 49:2240
23. Iribarne JV, Thompson BA. 1976. *J. Chem. Phys.* 64:2287
24. Emmett MR, Caprioli RM. 1994. *J. Am. Soc. Mass Spectrom.* 5:605
25. Wilm MS, Mann M. 1994. *Int. J. Mass Spectrom. Ion Process.* 136:167
26. Muddiman DC, Null AP, Hannis JC. 1999. *Rapid Commun. Mass Spectrom.* 13: 1201
27. Scalf M, Westphall MS, Krause J, Kaufman SL, Smith LM. 1999. *Science* 283:194
28. Stephenson JL, McLuckey SA. 1998. *Anal. Chem.* 70:3533
29. Chen RD, Cheng XH, Mitchell DW, Hofstadler SA, Wu Q, et al. 1995. *Anal. Chem.* 67:1159
30. Chowdhury SK, Katta V, Chait BT. 1990. *J. Am. Chem. Soc.* 112:9012
31. Carbeck JD, Severs JC, Gao JM, Wu QY, Smith RD, Whitesides GM. 1998. *J. Phys. Chem. B* 102:10596
32. Schnier PD, Gross DS, Williams ER. 1995. *J. Am. Soc. Mass Spectrom.* 6:1086
33. Schnier PD, Price WD, Williams ER. 1996. *J. Am. Soc. Mass Spectrom.* 7:972

34. Comisarow MB, Marshall AG. 1974. *Chem. Phys. Lett.* 25:282
35. Hendrickson CL, Emmett MR. 1999. *Annu. Rev. Phys. Chem.* 50:517
36. Alford JM, Williams PE, Trevor DJ, Smalley RE. 1986. *Int. J. Mass Spectrom. Ion Process.* 72:33
37. McIver RT, Hunter RL, Bowers WD. 1985. *Int. J. Mass Spectrom. Ion Process.* 64: 67
38. Kofel P, Alleman M, Kellerhals H, Wancek KP. 1985. *Int. J. Mass Spectrom. Ion Process.* 65:97
39. Dunbar RC, McMahon TB, Tholmann D, Tonner DS, Salahub DR, Wei DQ. 1995. *J. Am. Chem. Soc.* 117:12819
40. Dunbar RC, McMahon TB. 1998. *Science* 279:194
41. Price WD, Schnier PD, Jockrush RA, Strittmatter EF, Williams ER. 1996. *J. Am. Chem. Soc.* 118:10640
42. Reimann CT, Quist AP, Kopniczky J, Sundqvist BUR, Erlandsson R, Tengvall P. 1994. *Nucl. Instrum. Methods B* 88:29
43. Quist AP, Ahlbom J, Reimann CT, Sundqvist BUR. 1994. *Nucl. Instrum. Methods B* 88:164
44. Sullivan PA, Axelsson J, Altman S, Quist AP, Sundqvist BUR, Reimann CT. 1995. *J. Mass Spectrom.* 7:329
45. Covey TR, Douglas DJ. 1993. *J. Am. Soc. Mass Spectrom.* 4:616
46. Douglas DJ. 1994. *J. Am. Soc. Mass Spectrom.* 5:17
47. Collings BA, Douglas DJ. 1996. *J. Am. Chem. Soc.* 118:4488
48. Cox KA, Julian RK, Cooks RG, Kaiser RE. 1994. *J. Am. Soc. Mass Spectrom.* 5:127
49. Revercomb HE, Mason EA. 1997. *Anal. Chem.* 47:970
50. Dugourd Ph, Hudgins RR, Clemmer DE, Jarrold MF. 1997. *Rev. Sci. Instrum.* 68: 1122
51. Hudgins RR, Woenckhaus J, Jarrold MF. 1997. *Int J. Mass Spectrom. Ion Process.* 165/166:497
52. Mack E. 1925. *J. Am. Chem. Soc.* 47:2468
53. Hare WE, Mack E. 1932. *J. Am. Chem. Soc.* 54:4272
54. Hagen DF. 1979. *Anal. Chem.* 51:870
55. Karpas Z, Stimac RM, Rappoport Z. 1988. *Int. J. Mass Spectrom. Ion Process.* 83:163
56. Von Helden G, Hsu M-T, Kemper PR, Bowers MT. 1991. *J. Chem. Phys.* 95:3835
57. Von Helden G, Hsu M-T, Gotts N, Bowers MT. 1993. *J. Phys. Chem.* 97:8182
58. Mesleh MF, Hunter JM, Shvartsburg AA, Schatz GC, Jarrold MF. 1996. *J. Phys. Chem.* 100:16082
59. Shvartsburg AA, Jarrold MF. 1996. *Chem. Phys. Lett.* 261:86
60. Jarrold MF, Honea EC. 1992. *J. Am. Chem. Soc.* 114:459
61. Valentine SJ, Counterman AE, Hoagland CS, Reilly JP, Clemmer DE. 1998. *J. Am. Soc. Mass. Spectrom.* 9:1213
62. Srebalus CA, Li J, Marshall WS, Clemmer DE. 1999. *Anal. Chem.* 71:3918
63. Harrison AG. 1997. *Mass Spectrom. Rev.* 16:201
64. Hunter EPL, Lias SG. 1998. *J. Phys. Chem. Ref. Data* 27:413
65. Zhang K, Zimmerman DM, Chung-Phillips A, Cassady CJ. 1993. *J. Am. Chem. Soc.* 115:10812
66. Wu ZC, Fenselau C. 1993. *Tetrahedron* 49:9197
67. Wu JY, Lebrilla CB. 1993. *J. Am. Chem. Soc.* 115:3270
68. Carr SR, Cassady CJ. 1996. *J. Am. Soc. Mass Spectrom.* 7:1203
69. Wyttenbach T, Von Helden G, Bowers MT. 1996. *J. Am. Chem. Soc.* 118:8355
70. Suenram RD, Lovas FJ. 1978. *J. Mol. Spectrosc.* 72:272
71. Locke MJ, McIver RT. 1983. *J. Am. Chem. Soc.* 105:4226
72. Jensen JH, Gordon MS. 1995. *J. Am. Chem. Soc.* 117:8159
73. Rizzo TR, Park YD, Levy DH. 1986. *J. Chem. Phys.* 85:6945
74. Price WD, Jockusch RA, Williams ER. 1997. *J. Am. Chem. Soc.* 119:11988
75. Chapo CJ, Paul JB, Provencal RA, Roth

K, Saykally RJ. 1998. *J. Am. Chem. Soc.* 120:12956
76. Schnier PD, Price WD, Jockusch RA, Williams ER. 1996. *J. Am. Chem. Soc.* 118:7178
77. Campbell S, Rodgers MT, Marzluff EM, Beauchamp JL. 1995. *J. Am. Chem. Soc.* 117:12840
78. Lee S-W, Kim HS, Beauchamp JL. 1998. *J. Am. Chem. Soc.* 120:3188
79. Wyttenbach T, Bushnell JE, Bowers MT. 1998. *J. Am. Chem. Soc.* 120:5098
80. Rockwood AL, Busman M, Smith RD. 1991. *Int. J. Mass Spectrom. Ion Process.* 111:103
81. McLuckey SA, van Berkel GJ, Glish GL. 1990. *J. Am. Chem. Soc.* 112:5668
82. Wang XB, Wang LS. 1999. *Nature* 400:245
83. Cassady CJ, Carr SR. 1996. *J. Mass Spectrom.* 31:247
84. Valentine SJ, Counterman AE, Clemmer DE. 1997. *J. Am. Soc. Mass Spectrom.* 8:954
85. Gross DS, Williams ER. 1995. *J. Am. Chem. Soc.* 117:883
86. Gross DS, Rodriguez-Cruz SE, Bock S, Williams ER. 1995. *J. Phys. Chem.* 99:4034
87. Schnier PD, Gross DS, Williams ER. 1995. *J. Am. Chem. Soc.* 117:6747
88. Williams ER. 1996. *J. Mass Spectrom.* 31:831
89. Gronert S. 1996. *J. Am. Chem. Soc.* 118: 3525
90. Gronert S. 1999. *Int. J. Mass Spectrom.* 185–187:351
91. Zhang X, Cassady CJ. 1996. *J. Am. Soc. Mass Spectrom.* 7:1211
92. Miteva M, Demirev PA, Karshikoff AD. 1997. *J. Phys. Chem. B* 101:9645
93. Mao Y, Woenckhaus J, Kolafa J, Ratner MA, Jarrold MF. 1999. *J. Am. Chem. Soc.* 121:2712
94. Gilson MK, Honig B. 1986. *Biopolymers* 25:2097
95. Sharp KA, Honig B. 1990. *Annu. Rev. Biophys. Biophys. Chem.* 19:301
96. Warshel A, Åqvist J. 1991. *Annu. Rev. Biophys. Biophys. Chem.* 20:267
97. Shelimov KB, Clemmer DE, Hudgins RR, Jarrold MF. 1997. *J. Am. Chem. Soc.* 119:2240
98. Gross DS, Schnier PD, Rodriguez-Cruz SE, Fagerquist CK, Williams ER. 1996. *Proc. Natl. Acad. Sci. USA* 93:3143
99. Valentine SJ, Anderson J, Ellington AE, Clemmer DE. 1997. *J. Phys. Chem. B* 101:3891
100. Bakhtiar R, Wu Q, Hofstadler SA, Smith RD. 1994. *Biol. Mass Spectrom.* 23:707
101. Loo JA, Edmonds CG, Smith RD. 1988. *Rapid Commun. Mass Spectrom.* 2:207
102. Busman M, Rockwood AL, Smith RD. 1992. *J. Phys. Chem.* 96:2397
103. Senko MW, Speir JP, McLafferty FW. 1994. *Anal. Chem.* 66:2801
104. Little DP, Speir JP, Senko MW, O'Connor PB, McLafferty FW. 1994. *Anal. Chem.* 66:2809
105. Jockusch RA, Schnier PD, Price WD, Strittmatter EF, Demirev PA, Williams ER. 1997. *Anal. Chem.* 69:1119
106. Barbacci DC, Russell DH. 1999. *J. Am. Soc. Mass Spectrom.* 10:1038
107. Tsaprailis G, Nair H, Somogyi A, Wysocki VH, Zhong W, et al. 1999. *J. Am. Chem. Soc.* 121:5142
108. Zubarev RA, Kruger NA, Fridriksson EK, Lewis MA, Horn DM, et al. 1999. *J. Am. Chem. Soc.* 121:2857
109. Yu W, Vath JE, Huberty MC, Martin SA. 1993. *Anal. Chem.* 65:3015
110. Loo JA, Edmonds CG, Smith RD. 1993. *Anal. Chem.* 65:425
111. Ishikawa K, Nishimura T, Koga Y, Niwa Y. 1994. *Rapid Commun. Mass Spectrom.* 8:933
112. Roder H, Elösve GA, Englander SW. 1988. *Nature* 335:700
113. Englander SW. 1993. *Science* 262:848
114. Winger BE, Light-Wahl KJ, Rockwood AL, Smith RD. 1992. *J. Am. Chem. Soc.* 114:5897
115. Suckau D, Shi Y, Beu SC, Senko MW,

Quinn JP, et al. 1993. *Proc. Natl. Acad. Sci. USA* 90:790
116. Wood TD, Chorush RA, Wampler FM, Little DP, O'Connor PB, McLafferty FW. 1995. *Proc. Natl. Acad. Sci. USA* 92:2451
117. Valentine SJ, Clemmer DE. 1997. *J. Am. Chem. Soc.* 119:3558
118. McLafferty FW, Guan Z, Haupts U, Wood TD, Kelleher NL. 1998. *J. Am. Chem. Soc.* 120:4732
119. Freitas MA, Hendrickson CL, Emmett MR, Marshall AG. 1999. *Int J. Mass Spectrom.* 187–189:565
120. Wang F, Freitas MA, Marshall AG, Sykes BD. 1999. *Int. J. Mass Spectrom.* 192:319
121. Gard E, Green MK, Bregar J, Lebrilla CB. 1994. *J. Am. Soc. Mass Spectrom.* 5:623
122. Green MK, Lebrilla CB. 1998. *Int. J. Mass Spectrom. Ion Process.* 175:15
123. Campbell S, Rodgers MT, Marzluff EM, Beauchamp JL. 1994. *J. Am. Chem. Soc.* 116:9765
124. Wyttenbach T, Bowers MT. 1999. *J. Am. Soc. Mass Spectrom.* 10:9
125. Freitas MA, Marshall AG. 1999. *Int. J. Mass Spectrom.* 183:221
126. Stephenson JL, Schaaff TG, McLuckey SA. 1999. *J. Am. Soc. Mass Spectrom.* 10:552
127. Shelimov KB, Jarrold MF. 1996. *J. Am. Chem. Soc.* 118:10313
128. Shelimov KB, Jarrold MF. 1997. *J. Am. Chem. Soc.* 119:2987
129. Reimann CT, Velazquez I, Tapia O. 1998. *J. Phys. Chem. B* 102:2277
130. Reimann CT, Velazquez I, Tapia O. 1998. *J. Phys. Chem. B* 102:9344
131. Arteca GA, Velazquez I, Reimann CT, Tapia O. 1999. *J. Chem. Phys.* 111:4774
132. Arteca GA, Velazquez I, Reimann CT, Tapia O. 1999. *Phys. Rev. E* 59:5981
133. Mao Y, Ratner MA, Jarrold MF. 1999. *J. Phys. Chem. B* 103:10017
134. Alonso DO, Daggett V. 1998. *Protein Sci.* 7:860
135. Chakrabartty A, Baldwin RL. 1995. *Adv. Protein Chem.* 46:141
136. Blanco FJ, Rivas G, Serrano L. 1994. *Nat. Struct. Biol.* 1:584
137. Kaltashov IA, Feneslau C. 1997. *Proteins Struct. Funct. Genet.* 27:165
138. Li A, Feneslau C, Kaltashov IA. 1998. *Proteins Struct. Funct. Genet. Suppl.* 2:22
139. Ramirez-Alvarado M, Blanco FJ, Serrano L. 1996. *Nat. Struct. Biol.* 3:604
140. Ilyina E, Roongta V, Mayo KH. 1997. *Biochemistry* 36:5245
141. Hudgins RR, Mao Y, Ratner MA, Jarrold MF. 1999. *Biophys. J.* 76:1591
142. Samuelson S, Martyna G. 1999. *J. Chem. Phys.* 103:1752
143. Hudgins RR, Ratner MA, Jarrold MF. 1998. *J. Am. Chem. Soc.* 120:12974
144. Hudgins RR, Jarrold MF. 1999. *J. Am. Chem. Soc.* 121:3494
145. Hudgins RR, Jarrold MF. 2000. *J. Phys. Chem B.* 104:2154
146. Valentine SJ, Counterman AE, Clemmer DE. 1999. *J. Am. Soc. Mass Spectrom.* 10:1188
147. Lau YK, Ikuta S, Kebarle P. 1986. *J. Am. Chem. Soc.* 104:1462
148. Chowdhury SK, Katta V, Chait BT. 1990. *Rapid Commun. Mass Spectrom.* 4:81
149. Rodriguez-Cruz SE, Klassen JS, Williams ER. 1997. *J. Am. Soc. Mass Spectrom.* 8:565
150. Rodriguez-Cruz SE, Klassen JS, Williams ER. 1999. *J. Am. Soc. Mass Spectrom.* 10:958
151. Lee S-W, Freivogel P, Schindler T, Beauchamp JL. 1998. *J. Am. Chem. Soc.* 120:11758
152. Wei S, Shi Z, Castleman AW. 1991. *J. Chem. Phys.* 94:3268
153. Kuntz ID, Kauzmann W. 1974. *Adv. Protein Chem.* 28:239
154. Rupley JA, Careri G. 1991. *Adv. Protein Chem.* 41:37
155. Klassen JS, Blades AT, Kebarle P. 1995. *J. Phys. Chem.* 99:15509
156. Zhan D, Rosell J, Fenn JB. 1998. *J. Am. Soc. Mass Spectrom.* 9:1241
157. Woenckhaus J, Mao Y, Jarrold MF.

1997. *J. Phys. Chem. B* 101:847
158. Woenckhaus J, Hudgins RR, Jarrold MF. 1997. *J. Am. Chem. Soc.* 119:9586
159. Wlodawer A, Nachman J, Gilliland GL, Gallagher W, Woodward C. 1987. *J. Mol. Biol.* 198:469
160. Otting G, Wüthrich K. 1989. *J. Am. Chem. Soc.* 111:1871
161. Mao Y, Ratner MA, Jarrold MF. 2000. *J. Am. Chem. Soc.* 122:2950
162. Fye JL, Woenckhaus J, Jarrold MF. 1998. *J. Am. Chem. Soc.* 120:1327
163. Lee B, Richards FM. 1971. *J. Mol. Biol.* 55:379
164. Theorell H, Åkesson Å. 1941. *J. Am. Chem. Soc.* 63:1818